Acta Cryst E CRYSTALLOGRAPHIC COMMUNICATIONS

ISSN 2056-9890

catena-Poly[[bis(diaqualithium)]-μ_4-3,3′,5,5′-tetranitro-4,4′-bipyrazole-1,1′-diido]: a new moisture-insensitive alkali-metal energetic salt with a well-defined network structure

Kostiantyn V. Domasevitch,[a]* Ganna A. Senchyk[a] and Harald Krautscheid[b]

[a]Inorganic Chemistry Department, National Taras Shevchenko University of Kyiv, Volodymyrska Str. 64/13, 01601 Kyiv, Ukraine, and [b]Institute of Inorganic Chemistry, Leipzig University, Johannisallee 29, D-04103 Leipzig, Germany. *Correspondence e-mail: dk@univ.kiev.ua

Received 2 June 2023
Accepted 14 June 2023

Edited by S. Parkin, University of Kentucky, USA

Keywords: crystal structure; lithium; nitropyrazoles; energetic materials; hydrogen bonding.

CCDC reference: 2269963

Supporting information: this article has supporting information at journals.iucr.org/e

In the structure of the title salt, $[Li_2(C_6N_8O_8)(H_2O)_4]_n$, the 3,3′,5,5′-tetranitro-4,4′-bipyrazole-1,1′-diide dianion [{TNBPz}$^{2-}$] is situated across the twofold axis. The distorted coordination octahedra around Li^+ involve four short bonds with two pyrazolate N atoms and two aqua ligands [Li—N(O) = 1.999 (3)–2.090 (2) Å] and two longer contacts with nitro-O atoms [2.550 (2), 2.636 (2) Å]. When combined with μ_4-{TNBPz}$^{2-}$, this generates a mono-periodic polymeric structure incorporating discrete centrosymmeric [$(H_2O)_2$Li–(dinitropyrazolato)$_2$–Li$(H_2O)_2$] units. The three-dimensional stack of mutually orthogonal coordination chains is reminiscent of a Lincoln log pattern. It is influenced by conventional hydrogen bonding [O···O = 2.8555 (17)–3.0010 (15) Å] and multiple lone pair–π hole interactions of the nitro groups [N···O = 3.0349 (15) and 3.0887 (15) Å]. The Hirshfeld surface and two-dimensional fingerprint plots also support the significance of non-covalent bonding. Coordinative saturation and a favorable geometry at the Li^+ ions, dense packing of the polymeric subconnectivities and particularly extensive interanion interactions may be involved in the stabilization of the structure. The title salt is a rare example of an energetic Li nitroazolate, which nicely crystallizes from aqueous solution and is neither hygroscopic nor efflorescent. The TG/DTA data reveal total dehydration in the range of 330–430 K and stability of the anhydrous material up to 633–653 K.

1. Chemical context

Red-light-emitting technical or military pyrotechnics traditionally concern the utilization of Sr salts (Sabatini, 2018). However, there is a growing interest for alternative red-flame colorants since strontium is potentially harmful to human health, specifically replacing calcium in bone and affecting skeletal development (Glück *et al.*, 2017). Recent works by Klapötke suggest significant potential for lithium-based systems, in particular those incorporating energetic nitropyrazole species (Dufter-Münster *et al.*, 2022; Dufter *et al.*, 2020). The accumulation of nitro groups enhances acidity (pK_a = 3.14 for 3,5-dinitropyrazole *vs* 14.63 for the parent pyrazole; Janssen *et al.*, 1973) for producing hydrolytically stable salts, while the incorporation of energy-rich nitropyrazolates contributes to oxygen balance of the formulations. In addition, the high nitrogen content and N—N linkage within the pyrazole ring inherently facilitate the release of nitrogen gas when burned. This meets the needs for cooling the flame for improving the color purity (Glück *et al.*, 2017).

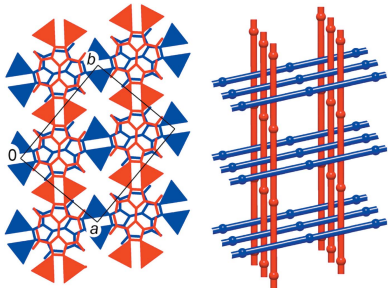

However, most of the examined salts are still not suited for applications in spite of such valuable pre-requisites. The nitropyrazolates crystallize with difficulty (Drukenmüller *et al.*, 2014) and their Li salts are commonly hygroscopic and deliquescent (Dufter-Münster *et al.*, 2022). In the present work, we address this problem with a crystal-engineering approach. The recently introduced bifunctional tecton 3,3′,5,5′-tetranitro-4,4′-bipyrazole [H_2(TNBPz)] readily affords a range of salts with alkali metal ions (Domasevitch & Ponomarova, 2021) and nitrogen bases (Gospodinov *et al.*, 2020) and supports either coordination or hydrogen-bonded arrays in a very predictable fashion. One can anticipate that the doubled nitropyrazolate functionality could grant the connection of the Li^+ ions and generation of a relatively robust polymer, whereas the extended molecular framework of $\{TNBPz\}^{2-}$ is particularly beneficial for the dense anion–anion interactions because of a larger contribution of dispersion forces. An appropriate set of binding sites for such interactions may be found with four NO_2 functions, which commonly act as self-complementary donor and acceptor groups for non-covalent lone pair–π hole bonds (Bauzá *et al.*, 2017). With this in mind, we prepared the new energetic salt *catena*-poly[[bis(diaqualithium)]-μ_4-3,3′,5,5′-tetranitro-4,4′-bipyrazole-1,1′-diido] and report its structure here.

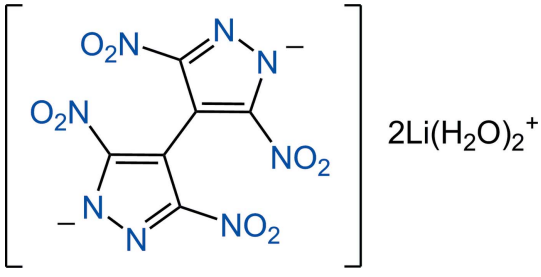

2. Structural commentary

The molecular structure of the title compound is shown in Fig. 1, with the asymmetric unit comprising one metal ion, two aqua ligands and half a molecule of the organic dianion $\{TNBPz\}^{2-}$, which is situated across the twofold axis passing through the center of the C—C bond between two pyrazole rings.

The coordination around the Li^+ ion may be regarded as distorted octahedral, with four relatively short bonds with two pyrazole-N atoms [2.086 (2) and 2.090 (2) Å], two aqua-O atoms [1.999 (3) and 2.027 (3) Å] and two elongated bonds with nitro-O atoms [2.550 (2) and 2.636 (2) Å] (Table 1). A very comparable pattern for lithium 4-amino-3,5-dinitropyrazolate retained only one Li—O(nitro) bond, which was slightly shorter [2.441 (4) Å; Dufter-Münster *et al.*, 2022]. Although the distorted octahedral geometries themselves are well known for Li^+ (Olsher *et al.*, 1991), the spread of the bond lengths is usually narrower. For example, the citrate salt exhibits six Li—O bonds in the range of 1.998 (2)–2.222 (3) Å (Rossi *et al.*, 1983). The exceedingly long bonds with nitro groups may be described rather as very weak ion-dipole

Table 1
Selected geometric parameters (Å, °).

Li1—O5	1.999 (3)	Li1—N2^{i}	2.090 (2)
Li1—O6	2.027 (3)	Li1—O3^{i}	2.550 (2)
Li1—N1	2.086 (2)	Li1—O1	2.636 (2)
O5—Li1—O6	145.63 (13)	N1—Li1—O3^{i}	170.20 (11)
O5—Li1—N1	98.49 (10)	N2^{i}—Li1—O3^{i}	68.60 (7)
O6—Li1—N1	101.69 (11)	O5—Li1—O1	80.47 (8)
O5—Li1—N2^{i}	100.84 (11)	O6—Li1—O1	81.94 (9)
O6—Li1—N2^{i}	101.22 (11)	N1—Li1—O1	67.50 (7)
N1—Li1—N2^{i}	103.29 (10)	N2^{i}—Li1—O1	170.76 (11)
O5—Li1—O3^{i}	78.28 (8)	O3^{i}—Li1—O1	120.49 (9)
O6—Li1—O3^{i}	85.66 (8)		

Symmetry code: (i) $-x+1, -y+1, -z$.

contacts, while the remaining four shorter bonds almost perfectly match the sum of the corresponding ionic radii for 4-coordinate Li^+ ions [which are Li—O = 1.94 Å and Li—N = 2.05 Å; Shannon, 1976]. Nevertheless, the weak Li—O(nitro) interactions are presumably important for a more effective shielding of the cations against hydration when exposed to moist air. Unlike many related systems, crystals of the title compound are not hygroscopic. A second issue is the saturation of the Li^+ environment with an appropriate number of aqua ligands. This is contrary to the structures of far more moisture-sensitive 3,4-, 3,5-dinitropyrazolates and 4-amino-3,5-dinitropyrazolate, where the diaqualithium moieties were recognized as local fragments of 1:1 aqualithium chains –Li–[(μ-H_2O)Li]$_n$– (Dufter-Münster *et al.*, 2022).

The geometric parameters of the $\{TNBPz\}^{2-}$ dianion are consistent with the data for neutral H_2(TNBPz) (Domasevitch *et al.*, 2019) or singly charged species $\{H(TNBPz)\}^{-}$ (Domasevitch & Ponomarova, 2021). The ion adopts a twisted conformation with two pyrazole rings rotated by 54.48 (4)° (Fig. 1). Although this twist is larger than 42.99 (8)° for Rb{H(TNBPz)} (Domasevitch & Ponomarova, 2021), it is still unusually small, as may be compared with the even less

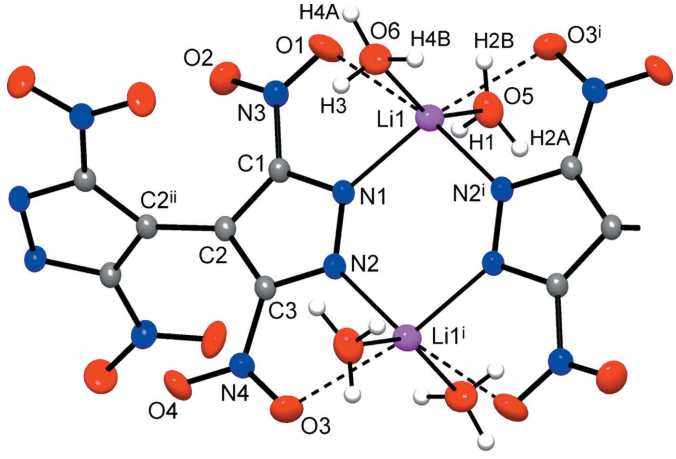

Figure 1
The molecular structure of the title compound with displacement ellipsoids drawn at the 50% probability level. Dotted lines indicate distal Li—O(nitro) interactions. Two out of four H atoms of the aqua ligands are equally disordered over two positions (H2*A*, H2*B* and H4*A*, H4*B*). [Symmetry codes: (i) $-x+1, -y+1, -z$; (ii) $-x+\frac{1}{2}, -y+\frac{1}{2}, z$.]

Table 2
Hydrogen-bond geometry (Å, °).

D—H···A	D—H	H···A	D···A	D—H···A
O5—H1···O4^{ii}	0.87 (2)	2.02 (2)	2.8818 (14)	174 (2)
O5—H2A···O2^{iii}	0.87 (2)	2.13 (2)	3.0010 (15)	177 (4)
O5—H2B···O6^{iv}	0.87 (2)	2.02 (2)	2.8555 (17)	163 (3)
O6—H3···O1^{v}	0.82 (3)	2.24 (3)	2.9995 (17)	153 (2)
O6—H4A···O6^{vi}	0.92 (4)	2.01 (4)	2.905 (2)	163 (4)
O6—H4B···O5^{vii}	0.95 (5)	1.93 (5)	2.8555 (17)	164 (4)

Symmetry codes: (ii) $-x+\frac{1}{2}, y, z+\frac{1}{2}$; (iii) $-x+1, y+\frac{1}{2}, -z+\frac{1}{2}$; (iv) $-x+\frac{3}{2}, y, z+\frac{1}{2}$; (v) $x, -y+\frac{1}{2}, z-\frac{1}{2}$; (vi) $-x+\frac{3}{2}, -y+\frac{1}{2}, z$; (vii) $-x+\frac{3}{2}, y, z-\frac{1}{2}$.

hindered 3,3′,5,5′-tetramethyl-4,4′-bipyrazole analogs (65–90°; Ponomarova *et al.*, 2013). In fact, the intramolecular interactions of NO_2 groups, with a shortest contact N3···O4^{ii} = 2.9199 (15) Å [symmetry code: (ii) $-x+\frac{1}{2}, -y+\frac{1}{2}, z$], are likely attractive, as a kind of lone pair–π hole bonding (Bauzá *et al.*, 2017). The central C2—C2^{ii} bond is insensitive to the protolytic effects [1.463 (2) Å *vs* 1.4644 (15) and 1.462 (2) Å for H_2(TNBPz) and Rb{H(TNBPz)}, respectively], which indicates a lack of essential conjugation between two pyrazolate rings. Shortening of the C-NO_2 bonds upon deprotonation is also minor [mean 1.4308 (16) Å *vs* 1.439 (2) Å for H_2(TNBPz)], while a certain increase in conjugation is reflected rather by a perceptible flattening of the dinitropyrazole fragments. For the latter, the NO_2 groups are nearly coplanar with the ring, the two dihedral angles are 1.35 (8) and 11.66 (8)°, for N4O3O4 and N3O1O2 groups, respectively. In the case of H_2(TNBPz), the twist comes to 22.8 (2)°. The most appreciable consequence of the dianionic structure is similarity of bond angles at the ring-N atoms: N2—N1—C1 = 107.11 (9)° and N1—N2—C3 = 106.93 (9)°. For the neutral dinitropyrazole rings, the parameters for N- [103.9 (2)°] and NH-sites [112.0 (2)°] are clearly different (Domasevitch *et al.*, 2019).

3. Supramolecular features

The title compound adopts a mono-periodic polymeric structure with the {TNBPz}$^{2-}$ anions acting as tetradentate bridging ligands. Two dinitropyrazolate groups of the anions and two diaqualithium fragments compose the cyclic pattern (Fig. 2), which is reminiscent of the dimers in lithium 3,5-dinitro-4-amino- and 3,4-dinitropyrazolates (Dufter-Münster *et al.*, 2022). Unlike these monofunctional prototypes, with the C2—C2^{ii} bond linking the two pz halves of the bipyrazole core, these dimers are connected into linear chains, with a distance of 9.06 Å between the centroids of the $Li_2(pz)_2$ cycles (pz is pyrazole).

Adjacent chains are linked by a set of conventional hydrogen bonds O—H···O, which involve either aqua or nitro-O acceptors. The geometric parameters for five types of such interactions are very comparable (Table 2), with the range of O···O separations [2.8555 (17)–3.0010 (15) Å] and nearly straight angles at the H atoms [153 (2)–177 (4)°] indicating directional hydrogen bonding. Bonds of the type O6—H4A···O6^{vii} [symmetry code: (vii) $-x+\frac{3}{2}, -y+\frac{1}{2}, z$; the H atom is equally disordered over two symmetry-related O atoms] are important for the connection of the chains into layers, which are parallel to the *ab* plane, whereas the second aqua/aqua bond O5—H···O6^{v} [symmetry code: (v) $-x+\frac{3}{2}, y, z+\frac{1}{2}$] and all three aqua/nitro hydrogen bonds actualize between the layers (Fig. 3).

The coordination chains of two successive layers are inclined, one in relation to the other, and adopt an angle of 78.9° [which is the angle between the (110) and ($\bar{1}$10) directions in the crystal]. This nearly orthogonal mutual orientation conditions a very simple packing pattern, in the form of Lincoln log-like stacks (Fig. 2). The {TNBPz}$^{2-}$ anions are situated exactly one on the top of the other at the distances of 4.71 Å corresponding to one half of the *c* parameter of the unit

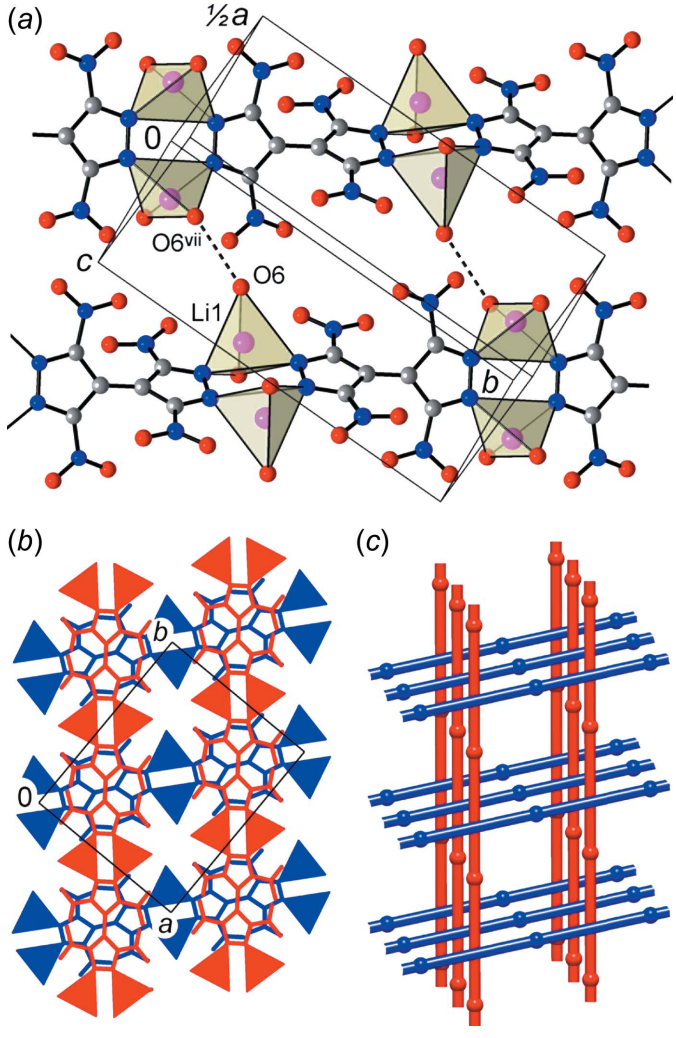

Figure 2
(*a*) View of the coordination chains with hydrogen-bond interactions between pairs of symmetry-related aqua ligands that afford layers parallel to the *ab* plane. The Li^+ ions are represented by coordination tetrahedra, while considering only the four shortest coordination bonds. (*b*) Projection of the structure on the *ab* plane with two successive layers indicated in blue and red. (*c*) Packing of the coordination chains following a Lincoln log pattern. The chain nodes represent the dilithium units and the chain links are bridging {TNBPz}$^{2-}$ anions. [Symmetry code: (vii) $-x+\frac{3}{2}, -y+\frac{1}{2}, z$.]

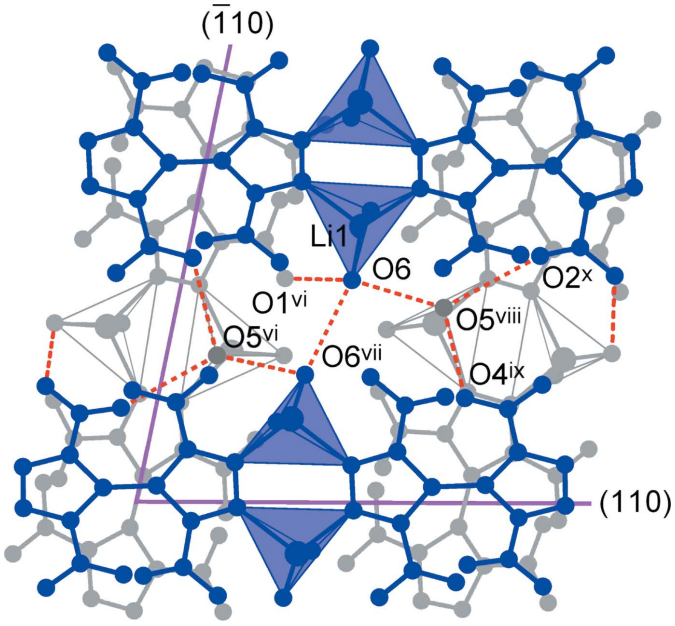

Figure 3
The hydrogen bonding between adjacent coordination chains, which is shown by the dotted red lines. Two successive layers are marked in blue and gray and the Li^+ ions are presented as coodination tetrahedra, while considering only the four shortest coordination bonds for clarity. The purple lines identify the directions of the coordination chains, which coincide with the crystal directions (110) and ($\bar{1}$10). [Symmetry codes: (vi) $x, -y+\frac{1}{2}, z-\frac{1}{2}$; (vii) $-x+\frac{3}{2}, -y+\frac{1}{2}, z$; (ix) $x+1, y, z$; (x) $x+\frac{1}{2}, y+\frac{1}{2}, -z$.]

cell. In spite of the twisted conformation of the bipyrazole, such stacking is geometrically favorable, with every pair of molecules within the stack mutually fitting like puzzles. The resulting interactions are particularly extensive, with four pairs of symmetry-related short contacts N3···O4^{iii} = 3.0349 (15) Å and N2···O2^{vi} = 3.0887 (15) Å [symmetry codes: (iii) $-x+\frac{1}{2}, y, z+\frac{1}{2}$; (vi) $x, -y+\frac{1}{2}, z-\frac{1}{2}$] established by every $\{TNBPz\}^{2-}$ anion (Fig. 4). For the mutually bonded nitro groups, *i.e.* N3O1O2 and (N4O3O4)^{iii}, the latter is lone-pair donor and the former one is π-hole acceptor, which combine to create a very characteristic stack (Veluthaparambath *et al.*, 2023). The planes of the two groups subtend a dihedral angle of 34.16 (15)°, but the N3···O4^{iii} axis is nearly orthogonal to the acceptor plane, as indicated by a slippage angle of 8.6 (2)°. The second type of interaction of is a lone pair–π-hole bond with the dinitropyrazolate ring system. Similar interactions are well known for electron-deficient N-heterocycles and they are most pronounced for 1,2,4,5-tetrazines (Gural'skiy *et al.*, 2009). In this case, the interplanar [49.96 (10)°] and slippage angles [13.98 (15)°, with respect to the centroid of the pyrazole ring] are slightly larger. This non-covalent bonding is clearly traced in every structure adopted by H_2(TNBPz) [with very short mutual nitro contacts down to N···O = 2.9115 (15) Å; Domasevitch *et al.*, 2019] and its anions (Domasevitch & Ponomarova, 2021) and in fact it may be regarded as a prominent feature for the crystal chemistry of such systems. These close interactions of shape-complementary twisted molecules contribute to the relatively high packing index of 75.8%, which is at the top of the 65–75% range expected for organic solids (Dunitz, 1995).

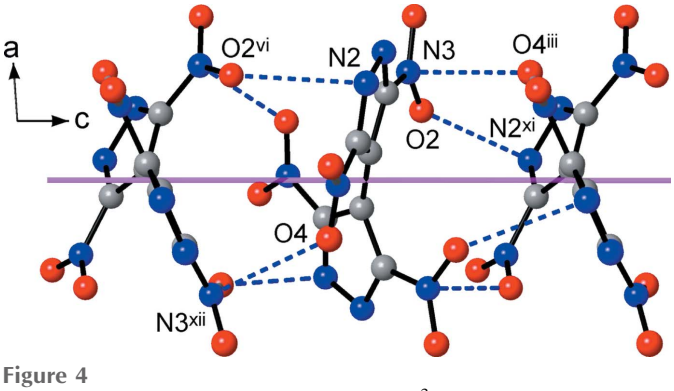

Figure 4
Lone pair-π–hole interactions of the $\{TNBPz\}^{2-}$ anions. The stacking axis is indicated by the purple line and it coincides with the *c*-axis direction. [Symmetry codes: (iii) $-x+\frac{1}{2}, y, z+\frac{1}{2}$; (vi) $x, -y+\frac{1}{2}, z-\frac{1}{2}$; (xi) $x, -y+\frac{1}{2}, z+\frac{1}{2}$; (xii) $-x+\frac{1}{2}, y, z-\frac{1}{2}$.]

4. Hirshfeld analysis

The supramolecular interactions in the title structure were further assessed by Hirshfeld surface analysis (Spackman & Byrom, 1997; McKinnon *et al.*, 2004; Hirshfeld, 1977; Spackman & McKinnon, 2002) performed with *CrystalExplorer17* (Turner *et al.*, 2017). The Hirshfeld surface of the individual $\{TNBPz\}^{2-}$ anion mapped over d_{norm}, using a fixed color scale of −0.73 (red) to 1.14 a.u. (blue), indicates a set of red spots associated with the interaction sites (Fig. 5). Two pairs of the most intense spots (−0.72 a.u.) are associated with the Li—N coordination, while the hydrogen bonding is also visualized as prominent features (−0.38 to −0.44 a.u.). The lone pair–π-hole interactions of NO_2 groups are less visible,

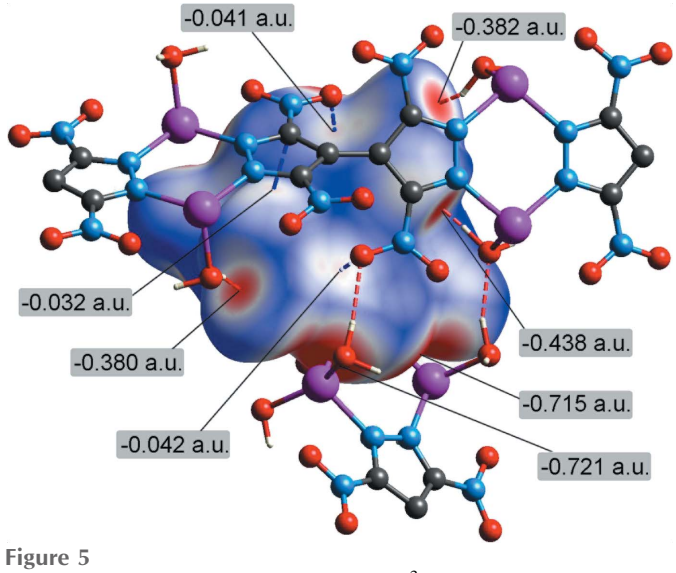

Figure 5
Hirshfeld surface of the individual $\{TNBPz\}^{2-}$ anion, mapped over d_{norm} (the C—H distances are normalized) in the color range −0.73 (red) to 1.14 a.u. (blue), with the red regions indicating the sites of intermolecular interactions.

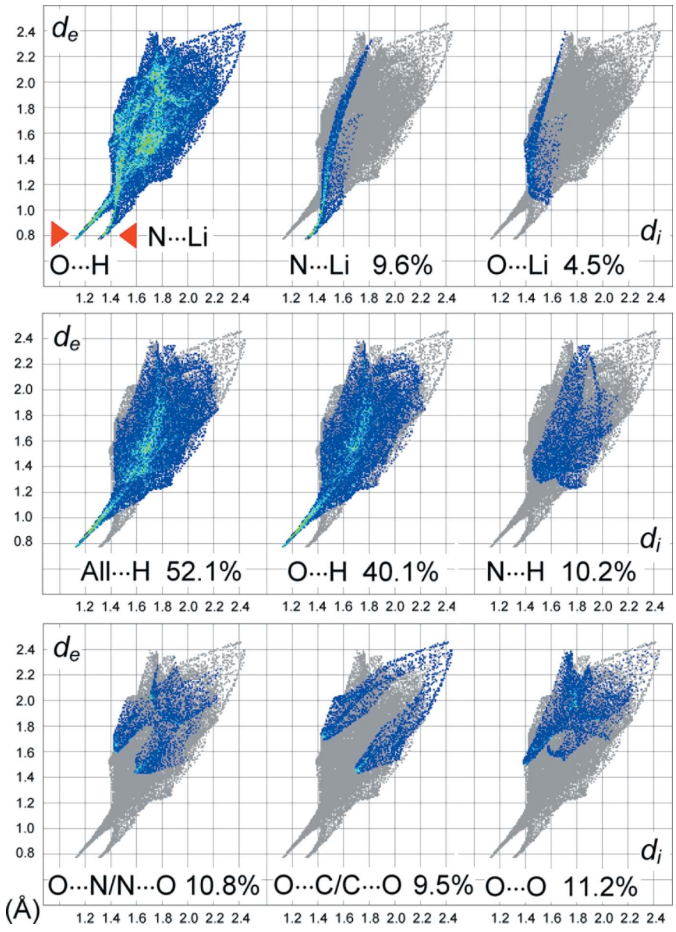

Figure 6
Two-dimensional fingerprint plots for the individual $\{TNBPz\}^{2-}$ anion, and delineated into the principal contributions of N···Li, O···Li, O···H, N···H, O···N/N···O, O···C/C···O and O···O contacts. Other contributors are: C···N/N···C, 1.8%; N···N, 0.5% and C···C, 0.1% contacts.

but they are still detectable on the surface as a set of very diffuse spots (−0.04 a.u.).

The two-dimensional fingerprint plots (Fig. 6) are even more informative. They suggest the significance of coordination and hydrogen-bonding interactions, which are reflected as two sharp spikes pointing to the lower left with the shortest contacts N···Li = 2.1 Å and O···H = 2.0 Å. One can note a similar indication of N···Li (9.6%) and O···Li (4.5%) contacts, but the fraction of the latter is significantly less and the corresponding short spike is diffuse. This agrees with the weakness of the coordination bonds adopted by the nitro-O atoms. O···H interactions account for 40.1% of the entire number of contacts. This is complemented by a 10.2% contribution of N···H contacts, but there are no signs of any O—H···N bonding. The plot represents a rather diffuse collection of points with the shortest N···H = 2.8 Å. The large fraction of O···N/N···O and O···C/C···O contacts (in total over 20%) is a primary indicator for extensive anion–anion interactions. The nature of these contacts is similar and they appear in the plots as nearly symmetrical (about the diagonal where $d_i = d_e$) pairs of features. Therefore, either donor or acceptor sites of the bonds are found within the individual anions supporting the shortest contacts O···N = 3.0 Å and O···C = 3.1 Å. It may be postulated that the accessibility of aqua hydrogen-bond donors does not disrupt the main anion–anion interactions, but rather governs elimination of less favorable nitro O···O contacts. The total contributions of the C(N)···C(N,O) contacts in the title structure and in the very similar unsolvated Rb{H(TNBPz)} (Domasevitch & Ponomarova, 2021) are nearly identical (33.4% and 31.9%, respectively), while the impact of hydrogen bonding is best illustrated by the pronounced contraction of the O···O fraction (37.4% to 11.2% in the present case). Moreover, the asymmetry of the O···O plot is contrary to the patterns for the O···N/N···O and O···C/C···O contacts. This witnesses the prevalence of the nitro/aqua contacts, instead of direct nitro O···O interactions.

5. Synthesis and crystallization

3,3′,5,5′-Tetranitro-4,4′-bipyrazole monohydrate $[H_2(TNBPz)\cdot H_2O]$ is readily available by nitration of 4,4′-bipyrazole in mixed acids (yield 92%) and subsequent crystallization from water (Domasevitch *et al.*, 2019).

For the preparation of the title compound, 0.294 g (7.0 mmol) of $LiOH\cdot H_2O$ was dissolved in 10 ml of water at 333–343 K and then 1.162 g (3.5 mmol) of solid $H_2(TNBPz)\cdot H_2O$ was added with stirring. The mixture was stirred for 30 min and the resulting clear deep-yellow solution was cooled to r.t. Slow evaporation to a minimum volume over 8–10 d led to crystallization of the product as well-developed large lemon-yellow prisms. The crystals were removed and dried on a filter paper in air. The yield was 1.25 g (90%). The material shows neither signs of hygroscopy nor efflorescence when exposed to ambient air for months.

Analysis (%) calculated for $C_6H_8Li_2N_8O_{12}$: C 18.10, H 2.03, N 28.15; found: C 18.45, H 1.99, N 28.42. IR (KBr, cm^{-1}): 564 *m*, 636 *m*, 698 *m*, 716 *m*, 773 *w*, 853 *s*, 1006 *m*, 1021 *s*, 1189 *w*, 1284 *w*, 1308 *s*, 1321 *s*, 1353 *s*, 1381 *s*, 1410 *s*, 1484 *s*, 1540 *s*, 1641 *m*, 1658 *m*, 3460 *br*, 3580 *br*.

The FT–IR spectrum reveals a distinctive pattern, which is characteristic for hydrated nitropyrazolates. The peaks, which are associated with the aqua ligands, appear at 3460 and 3580 cm^{-1} (O—H stretching), 1641, 1658 cm^{-1} (bend) and 564 cm^{-1} (libration). The peaks for symmetric and asymmetric NO_2 stretching (1351, 1381 and 1484, 1540 cm^{-1}, respectively) are very similar to the spectra of comparable 3,5-dinitropyrazole (Ravi, 2015). These double peaks originate in coupling of the NO_2 vibrations with the ring motions. The intense and sharp band at 853 cm^{-1} is ν(C—NO_2), and its shift, with respect to the band for $H_2(TNBPz)\cdot H_2O$ (839 cm^{-1}; Domasevitch *et al.*, 2019), suggests a certain increase of conjugation of the nitro groups with the carrier aromatic ring upon deprotonation. For Rb{H(TNBPz)}, both these frequencies were present (839 and 852 cm^{-1}; Domasevitch & Ponomarova, 2021).

Preliminary assays for safety of the title compound and its suitability for pyrotechnic formulations were performed by thermal analysis (OZM Research DTA 552-Ex). There are

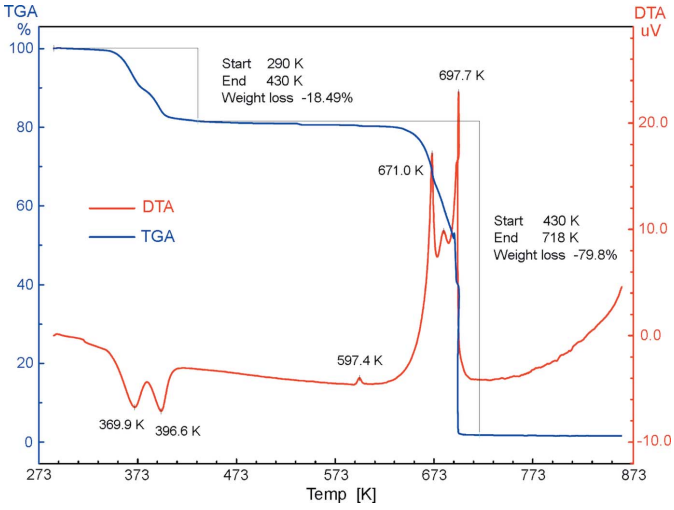

Figure 7
Combined DTA (red) and TGA (blue) plots for the title compound, in the temperature range of 273–873 K (air, heating rate 5 K min^{-1}).

two partially separated stages for nearly identical weight losses in the temperature range of 330–430 K (Fig. 7), which correspond to total dehydration of the salt (in total, −18.49 mass %; $-4H_2O$: calculated −18.09%). The anhydrous material is stable up to 633 K, with the very minor exothermic event at 597 K possibly indicating a phase transition. Exothermic decomposition proceeds above 653 K, with instantaneous loss of any remaining weight and a sharp exothermic effect at *ca* 700 K suggesting an explosion. For comparison, typical onset temperatures for decomposition of energetic Li nitropyrazolates are 400–500 K, and only 3,5-dinitropyrazolate is stable up to 600 K (Dufter-Münster *et al.*, 2022).

6. Refinement

Crystal data, data collection and structure refinement details are summarized in Table 3. The hydrogen atoms were located and then refined with isotropic thermal parameters. For both aqua ligands, one of the H atoms is equally disordered over two positions, which were refined with 0.5 partial contribution factors and with soft similarity restraints applied to O—H bond lengths [O—H = 0.82 (3)–0.95 (5) Å].

Table 3
Experimental details.

Crystal data	
Chemical formula	$[Li_2(C_6N_8O_8)(H_2O)_4]$
M_r	398.08
Crystal system, space group	Orthorhombic, *Pccn*
Temperature (K)	213
a, *b*, *c* (Å)	11.5094 (9), 13.9839 (8), 9.4247 (5)
V (Å^3)	1516.87 (17)
Z	4
Radiation type	Mo *Kα*
μ (mm^{-1})	0.17
Crystal size (mm)	0.25 × 0.22 × 0.20
Data collection	
Diffractometer	Stoe Image plate diffraction system
No. of measured, independent and observed [$I > 2\sigma(I)$] reflections	10855, 1817, 1225
R_{int}	0.049
$(\sin\theta/\lambda)_{max}$ (Å^{-1})	0.660
Refinement	
$R[F^2 > 2\sigma(F^2)]$, $wR(F^2)$, *S*	0.030, 0.072, 0.88
No. of reflections	1817
No. of parameters	151
No. of restraints	4
H-atom treatment	All H-atom parameters refined
$\Delta\rho_{max}$, $\Delta\rho_{min}$ (e Å^{-3})	0.28, −0.14

Computer programs: *IPDS Software* (Stoe & Cie, 2000), *SHELXS97* (Sheldrick, 2008), *SHELXL2014/7* (Sheldrick, 2015), Diamond (Brandenburg, 1999) and *WinGX* (Farrugia, 2012).

Funding information

This work was supported by the Ministry of Education and Science of Ukraine (Project No. 22BF037–11) and the National Research Foundation of Ukraine (Project No. 2020.02/0071).

References

Bauzá, A., Sharko, A. V., Senchyk, G. A., Rusanov, E. B., Frontera, A. & Domasevitch, K. V. (2017). *CrystEngComm*, **19**, 1933–1937.
Brandenburg, K. (1999). *DIAMOND*. Crystal Impact GbR, Bonn, Germany.
Domasevitch, K. V., Gospodinov, I., Krautscheid, H., Klapötke, T. M. & Stierstorfer, J. (2019). *New J. Chem.* **43**, 1305–1312.
Domasevitch, K. V. & Ponomarova, V. V. (2021). *Acta Cryst.* E**77**, 1109–1115.
Drukenmüller, I. E., Klapötke, T. M., Morgenstern, Y., Rusan, M. & Stierstorfer, J. (2014). *Z. Anorg. Allg. Chem.* **640**, 2139–2148.
Dufter, A. M. W., Klapötke, T. M., Rusan, M., Schweiger, A. & Stierstorfer, J. (2020). *ChemPlusChem*, **85**, 2044–2050.
Dufter-Münster, A. M. W., Harter, A. G., Klapötke, T. M., Reinhardt, E., Römer, J. & Stierstorfer, J. (2022). *Eur. J. Inorg. Chem.* e202101048.
Dunitz, J. D. (1995). *X-ray Analysis and the Structure of Organic Solids*, 2nd corrected reprint, pp. 106–111. Basel: Verlag Helvetica Chimica Acta.
Farrugia, L. J. (2012). *J. Appl. Cryst.* **45**, 849–854.
Glück, J., Klapötke, T. M., Rusan, M., Sabatini, J. J. & Stierstorfer, J. (2017). *Angew. Chem. Int. Ed.* **56**, 16507–16509.
Gospodinov, I., Domasevitch, K. V., Unger, C. C., Klapötke, T. M. & Stierstorfer, J. (2020). *Cryst. Growth Des.* **20**, 755–764.
Gural'skiy, I. A., Escudero, D., Frontera, A., Solntsev, P. V., Rusanov, E. B., Chernega, A. N., Krautscheid, H. & Domasevitch, K. V. (2009). *Dalton Trans.* pp. 2856–2864.
Hirshfeld, F. L. (1977). *Theor. Chim. Acta*, **44**, 129–138.
Janssen, J. W. A. M., Kruse, C. C., Koeners, H. J. & Habraken, C. (1973). *J. Heterocycl. Chem.* **10**, 1055–1058.
McKinnon, J. J., Spackman, M. A. & Mitchell, A. S. (2004). *Acta Cryst.* B**60**, 627–668.
Olsher, U., Izatt, R. M., Bradshaw, J. S. & Dalley, N. K. (1991). *Chem. Rev.* **91**, 137–164.
Ponomarova, V. V., Komarchuk, V. V., Boldog, I., Krautscheid, H. & Domasevitch, K. V. (2013). *CrystEngComm*, **15**, 8280–8287.
Ravi, P. (2015). *J. Mol. Struct.* **1079**, 433–447.
Rossi, M., Rickles, L. F. & Glusker, J. P. (1983). *Acta Cryst.* C**39**, 987–990.
Sabatini, J. J. (2018). *Prop. Explos. Pyrotech.* **43**, 28–37.
Shannon, R. D. (1976). *Acta Cryst.* A**32**, 751–767.
Sheldrick, G. M. (2008). *Acta Cryst.* A**64**, 112–122.
Sheldrick, G. M. (2015). *Acta Cryst.* C**71**, 3–8.

Spackman, M. A. & Byrom, P. G. A. (1997). *Chem. Phys. Lett.* **267**, 215–220.
Spackman, M. A. & McKinnon, J. J. (2002). *CrystEngComm*, **4**, 378–392.
Stoe & Cie (2000). *IPDS Software*. Stoe & Cie GmbH, Darmstadt, Germany.
Turner, M. J., McKinnon, J. J., Wolff, S. K., Grimwood, D. J., Spackman, P. R., Jayatilaka, D. & Spackman, M. A. (2017). *CrystalExplorer17*. University of Western Australia. http://crystalexplorer.scb.uwa.edu.au/.
Veluthaparambath, R. V. P., Krishna, V., Pancharatna, P. D. & Saha, B. K. (2023). *Cryst. Growth Des.* **23**, 442–449.

supporting information

Acta Cryst. (2023). E**79**, 657-663 [https://doi.org/10.1107/S2056989023005339]

catena-Poly[[bis(diaqualithium)]-μ_4-3,3′,5,5′-tetranitro-4,4′-bipyrazole-1,1′-diido]: a new moisture-insensitive alkali-metal energetic salt with a well-defined network structure

Kostiantyn V. Domasevitch, Ganna A. Senchyk and Harald Krautscheid

Computing details

Data collection: *IPDS Software* (Stoe & Cie, 2000); cell refinement: *IPDS Software* (Stoe & Cie, 2000); data reduction: *IPDS Software* (Stoe & Cie, 2000); program(s) used to solve structure: *SHELXS97* (Sheldrick, 2008); program(s) used to refine structure: *SHELXL2014*/7 (Sheldrick, 2015); molecular graphics: Diamond 2.1e (Brandenburg, 1999); software used to prepare material for publication: *WinGX* 1.70.01 (Farrugia, 2012).

catena-Poly[[bis(diaqualithium)]-μ_4-3,3′,5,5′-tetranitro-4,4′-bipyrazole-1,1′-diido]

Crystal data

$[Li_2(C_6N_8O_8)(H_2O)_4]$
M_r = 398.08
Orthorhombic, *Pccn*
a = 11.5094 (9) Å
b = 13.9839 (8) Å
c = 9.4247 (5) Å
V = 1516.87 (17) Å^3
Z = 4
F(000) = 808
D_x = 1.743 Mg m^{-3}
Mo *Kα* radiation, λ = 0.71073 Å
Cell parameters from 8000 reflections
θ = 2.9–28.0°
μ = 0.17 mm^{-1}
T = 213 K
Prism, yellow
0.25 × 0.22 × 0.20 mm

Data collection

Stoe Image plate diffraction system diffractometer
φ oscillation scans
10855 measured reflections
1817 independent reflections
1225 reflections with $I > 2\sigma(I)$
R_{int} = 0.049
θ_{max} = 28.0°, θ_{min} = 2.9°
h = −15→15
k = −16→18
l = −12→11

Refinement

Refinement on F^2
Least-squares matrix: full
$R[F^2 > 2\sigma(F^2)]$ = 0.030
$wR(F^2)$ = 0.072
S = 0.88
1817 reflections
151 parameters
4 restraints
Primary atom site location: structure-invariant direct methods
Secondary atom site location: difference Fourier map
Hydrogen site location: difference Fourier map
All H-atom parameters refined
$w = 1/[\sigma^2(F_o^2) + (0.0455P)^2]$ where $P = (F_o^2 + 2F_c^2)/3$
$(\Delta/\sigma)_{max} < 0.001$
$\Delta\rho_{max}$ = 0.28 e Å^{-3}
$\Delta\rho_{min}$ = −0.14 e Å^{-3}

Special details

Geometry. All esds (except the esd in the dihedral angle between two l.s. planes) are estimated using the full covariance matrix. The cell esds are taken into account individually in the estimation of esds in distances, angles and torsion angles; correlations between esds in cell parameters are only used when they are defined by crystal symmetry. An approximate (isotropic) treatment of cell esds is used for estimating esds involving l.s. planes.

Fractional atomic coordinates and isotropic or equivalent isotropic displacement parameters (Å²)

	x	*y*	*z*	U_{iso}*/U_{eq}	Occ. (<1)
Li1	0.62380 (18)	0.42289 (16)	0.0859 (2)	0.0258 (5)	
O1	0.57465 (8)	0.25173 (7)	0.18668 (12)	0.0401 (3)	
O2	0.42324 (9)	0.16320 (7)	0.21808 (12)	0.0357 (3)	
O3	0.17428 (9)	0.50551 (7)	−0.11938 (11)	0.0341 (3)	
O4	0.08500 (8)	0.37055 (7)	−0.08988 (11)	0.0327 (3)	
O5	0.62403 (9)	0.45230 (8)	0.29341 (11)	0.0336 (3)	
O6	0.69704 (11)	0.34427 (9)	−0.07111 (14)	0.0361 (3)	
N1	0.44846 (8)	0.38814 (7)	0.06362 (11)	0.0196 (2)	
N2	0.36602 (8)	0.43947 (7)	−0.00029 (12)	0.0191 (2)	
N3	0.47107 (9)	0.23391 (7)	0.16949 (12)	0.0236 (3)	
N4	0.17120 (9)	0.42244 (8)	−0.07765 (11)	0.0212 (2)	
C1	0.40259 (10)	0.30164 (9)	0.09198 (13)	0.0187 (3)	
C2	0.28824 (10)	0.29180 (9)	0.04627 (13)	0.0176 (3)	
C3	0.27171 (10)	0.38324 (8)	−0.01021 (13)	0.0178 (3)	
H1	0.5584 (14)	0.4317 (13)	0.327 (2)	0.071 (7)*	
H2A	0.608 (3)	0.5133 (13)	0.289 (4)	0.064 (13)*	0.5
H2B	0.671 (2)	0.409 (2)	0.326 (4)	0.047 (10)*	0.5
H3	0.651 (2)	0.3349 (17)	−0.136 (3)	0.089 (9)*	
H4A	0.724 (4)	0.284 (3)	−0.053 (4)	0.062 (13)*	0.5
H4B	0.749 (4)	0.390 (3)	−0.108 (5)	0.081 (15)*	0.5

Atomic displacement parameters (Å²)

	U^{11}	U^{22}	U^{33}	U^{12}	U^{13}	U^{23}
Li1	0.0233 (10)	0.0256 (12)	0.0285 (13)	−0.0004 (9)	0.0005 (9)	0.0042 (10)
O1	0.0233 (5)	0.0431 (6)	0.0540 (7)	−0.0006 (4)	−0.0134 (5)	0.0113 (5)
O2	0.0439 (6)	0.0233 (5)	0.0397 (6)	−0.0057 (4)	−0.0055 (5)	0.0132 (4)
O3	0.0329 (5)	0.0264 (5)	0.0431 (7)	0.0014 (4)	−0.0059 (4)	0.0133 (5)
O4	0.0219 (5)	0.0358 (6)	0.0406 (6)	−0.0075 (4)	−0.0109 (4)	0.0059 (5)
O5	0.0371 (6)	0.0374 (7)	0.0264 (6)	−0.0090 (5)	−0.0017 (5)	0.0036 (5)
O6	0.0336 (6)	0.0380 (7)	0.0369 (7)	0.0057 (5)	−0.0007 (5)	−0.0095 (5)
N1	0.0195 (5)	0.0176 (5)	0.0218 (6)	−0.0027 (4)	−0.0024 (4)	0.0020 (4)
N2	0.0190 (5)	0.0186 (5)	0.0197 (5)	−0.0032 (4)	0.0003 (4)	0.0014 (4)
N3	0.0257 (6)	0.0221 (6)	0.0229 (6)	−0.0016 (4)	−0.0038 (5)	0.0016 (5)
N4	0.0207 (5)	0.0226 (6)	0.0204 (6)	−0.0010 (4)	−0.0013 (4)	0.0016 (5)
C1	0.0187 (6)	0.0178 (6)	0.0195 (6)	−0.0028 (5)	−0.0011 (5)	0.0014 (5)
C2	0.0184 (6)	0.0178 (6)	0.0167 (6)	−0.0026 (5)	0.0008 (5)	−0.0013 (5)
C3	0.0177 (6)	0.0183 (6)	0.0174 (6)	−0.0021 (5)	−0.0006 (5)	−0.0007 (5)

Geometric parameters (Å, º)

Li1—O5	1.999 (3)	O5—H2B	0.866 (17)
Li1—O6	2.027 (3)	O6—H3	0.82 (3)
Li1—N1	2.086 (2)	O6—H4A	0.92 (4)
Li1—N2^{i}	2.090 (2)	O6—H4B	0.95 (5)
Li1—O3^{i}	2.550 (2)	N1—N2	1.3336 (14)
Li1—O1	2.636 (2)	N1—C1	1.3465 (16)
O1—N3	1.2287 (14)	N2—C3	1.3435 (15)
O2—N3	1.2209 (14)	N2—Li1^{i}	2.090 (2)
O3—N4	1.2270 (14)	N3—C1	1.4324 (16)
O3—Li1^{i}	2.550 (2)	N4—C3	1.4292 (16)
O4—N4	1.2346 (13)	C1—C2	1.3917 (16)
O5—H1	0.869 (15)	C2—C3	1.3981 (17)
O5—H2A	0.874 (17)	C2—C2^{ii}	1.463 (2)
O5—Li1—O6	145.63 (13)	H3—O6—H4A	102 (3)
O5—Li1—N1	98.49 (10)	Li1—O6—H4B	99 (3)
O6—Li1—N1	101.69 (11)	H3—O6—H4B	105 (3)
O5—Li1—N2^{i}	100.84 (11)	N2—N1—C1	107.11 (9)
O6—Li1—N2^{i}	101.22 (11)	N2—N1—Li1	127.46 (10)
N1—Li1—N2^{i}	103.29 (10)	C1—N1—Li1	124.64 (10)
O5—Li1—O3^{i}	78.28 (8)	N1—N2—C3	106.93 (9)
O6—Li1—O3^{i}	85.66 (8)	N1—N2—Li1^{i}	129.06 (9)
N1—Li1—O3^{i}	170.20 (11)	C3—N2—Li1^{i}	123.87 (10)
N2^{i}—Li1—O3^{i}	68.60 (7)	O2—N3—O1	123.53 (11)
O5—Li1—O1	80.47 (8)	O2—N3—C1	118.60 (10)
O6—Li1—O1	81.94 (9)	O1—N3—C1	117.84 (10)
N1—Li1—O1	67.50 (7)	O3—N4—O4	123.35 (11)
N2^{i}—Li1—O1	170.76 (11)	O3—N4—C3	118.83 (10)
O3^{i}—Li1—O1	120.49 (9)	O4—N4—C3	117.81 (10)
N3—O1—Li1	110.17 (9)	N1—C1—C2	113.46 (11)
N4—O3—Li1^{i}	111.00 (9)	N1—C1—N3	118.65 (10)
Li1—O5—H1	106.9 (14)	C2—C1—N3	127.80 (11)
Li1—O5—H2A	99 (3)	C1—C2—C3	98.98 (10)
H1—O5—H2A	99.0 (19)	C1—C2—C2^{ii}	130.38 (13)
Li1—O5—H2B	102 (2)	C3—C2—C2^{ii}	130.46 (12)
H1—O5—H2B	100.4 (19)	N2—C3—C2	113.51 (10)
Li1—O6—H3	111.1 (18)	N2—C3—N4	117.41 (10)
Li1—O6—H4A	121 (2)	C2—C3—N4	129.07 (10)
C1—N1—N2—C3	−0.25 (13)	N1—C1—C2—C3	−0.92 (14)
Li1—N1—N2—C3	169.92 (12)	N3—C1—C2—C3	175.50 (12)
C1—N1—N2—Li1^{i}	−176.01 (12)	N1—C1—C2—C2^{ii}	174.43 (9)
Li1—N1—N2—Li1^{i}	−5.8 (2)	N3—C1—C2—C2^{ii}	−9.15 (19)
Li1—O1—N3—O2	−173.04 (11)	N1—N2—C3—C2	−0.36 (14)
Li1—O1—N3—C1	4.91 (15)	Li1^{i}—N2—C3—C2	175.68 (11)
Li1^{i}—O3—N4—O4	−175.74 (11)	N1—N2—C3—N4	−179.10 (11)

Li1^{i}—O3—N4—C3	4.81 (14)	Li1^{i}—N2—C3—N4	−3.07 (17)
N2—N1—C1—C2	0.78 (14)	C1—C2—C3—N2	0.76 (14)
Li1—N1—C1—C2	−169.73 (11)	C2^{ii}—C2—C3—N2	−174.58 (10)
N2—N1—C1—N3	−175.99 (10)	C1—C2—C3—N4	179.32 (13)
Li1—N1—C1—N3	13.49 (18)	C2^{ii}—C2—C3—N4	4.0 (2)
O2—N3—C1—N1	166.52 (12)	O3—N4—C3—N2	−2.02 (17)
O1—N3—C1—N1	−11.53 (18)	O4—N4—C3—N2	178.50 (11)
O2—N3—C1—C2	−9.7 (2)	O3—N4—C3—C2	179.46 (12)
O1—N3—C1—C2	172.21 (13)	O4—N4—C3—C2	0.0 (2)

Symmetry codes: (i) −*x*+1, −*y*+1, −*z*; (ii) −*x*+1/2, −*y*+1/2, *z*.

Hydrogen-bond geometry (Å, º)

D—H···*A*	*D*—H	H···*A*	*D*···*A*	*D*—H···*A*
O5—H1···O4^{iii}	0.87 (2)	2.02 (2)	2.8818 (14)	174 (2)
O5—H2*A*···O2^{iv}	0.87 (2)	2.13 (2)	3.0010 (15)	177 (4)
O5—H2*B*···O6^{v}	0.87 (2)	2.02 (2)	2.8555 (17)	163 (3)
O6—H3···O1^{vi}	0.82 (3)	2.24 (3)	2.9995 (17)	153 (2)
O6—H4*A*···O6^{vii}	0.92 (4)	2.01 (4)	2.905 (2)	163 (4)
O6—H4*B*···O5^{viii}	0.95 (5)	1.93 (5)	2.8555 (17)	164 (4)

Symmetry codes: (iii) −*x*+1/2, *y*, *z*+1/2; (iv) −*x*+1, *y*+1/2, −*z*+1/2; (v) −*x*+3/2, *y*, *z*+1/2; (vi) *x*, −*y*+1/2, *z*−1/2; (vii) −*x*+3/2, −*y*+1/2, *z*; (viii) −*x*+3/2, *y*, *z*−1/2.